STUDYING COHERENT TRANSITION RADIATION SPATIAL IMAGE FEATURES FOR BUNCH LENGTH DIAGNOSTICS

A. Guisao-Betancur*[1,2], C. P. Welsch[1,2], J. Wolfenden†[1,2]
[1]University of Liverpool, Liverpool, UK
[2]Cockcroft Institute, Daresbury, UK

Abstract

Coherent transition radiation (CTR) has been widely used for developing diagnostics of particle beams due to its broadband spectrum, which provides information on the particle distribution, and its relatively simple experimental setup compared to other sources of coherent radiation. For short and ultrashort electron bunches, ps- to fs-long, methods such as CTR spectrometry and interferometry have been used. Recently, an alternative method using point-to-point spatial imaging of the transition radiation source plane has been studied, showing promising results in which image features, such as the image width, can be tied to the bunch length. However, a more in-depth image analysis is required. In this work, an attempt is made to model some of the bunch profile features from the CTR spatial images using conventional image and data analysis techniques. The CTR spatial images are simulated in Ansys Zemax OpticStudio for a broad range of bunch profiles, from single-Gaussian to multi-Gaussian distributions that emulate more realistic bunches. The results form the basis for the next stage of analysis of experimental CTR images for retrieving the longitudinal bunch profile.

INTRODUCTION

Diagnostics for ultrashort electron bunches pose challenges in plasma wakefield accelerators, as well as in short-pulse accelerators in general.

Time-domain methods, such as transverse deflecting structures, are the gold standard for longitudinal measurements down to the required sub-fs range in plasma accelerators [1], but they can be costly and may represent a significant footprint for future accelerators like EuPRAXIA or other plasma-based facilities, where size is an important factor. Transverse deflecting structures, however, are an intercepting diagnostic, which can make this method impractical for monitoring the bunch length at different positions along the beamline; thus, there is a need to develop alternative diagnostics that could potentially be compact and cost-efficient while achieving a similar resolution.

Instead of a time-domain technique, this study focuses on a monitor using polarization radiation [2], specifically coherent transition radiation (CTR). While other works have shown its use in characterizing ultrashort electron bunches via spectroscopy [3–5], the monitor studied in the present work uses point-to-point spatial imaging of the CTR source to determine longitudinal features of the bunch profile [6–8].

* A.M.Guisao-Betancur@liverpool.ac.uk
† joseph.wolfenden@cockcroft.ac.uk

CTR SPATIAL IMAGING

When assuming full transverse coherence of the bunch, that is, its rms transverse size $\sigma_r << \gamma\lambda/2\pi$ [5], the coherent power spectrum of the transition radiation will be given by:

$$S_{\mathrm{CTR}}(\rho(z),\omega) = S_p(\omega)N^2F_z(\rho(z),\omega)\,, \tag{1}$$

where $S_p(\omega)$ is the spectrum of a single-particle, N is the number of particles in the bunch, and $F_z(\rho(z),\omega)$ is the longitudinal form factor [9].

The particle distribution $\rho(z)$ (or the bunch profile) is contained in the longitudinal form factor, according to:

$$F_z(\rho(z),\omega) = \left|\int_{-\infty}^{\infty}\rho(z)e^{-i\frac{\omega}{c}z}dz\right|^2 . \tag{2}$$

The bunch profile $\rho(z)$ can be determined by measuring the spectrum and applying iterative phase methods [3–5]. But with CTR in particular, the focus of this work, there is another option to study the particle distribution by analyzing the image distribution for the particle bunch dI^i_{bunch}/dr [6,7]. This image corresponds to a point-to-point spatial image of the CTR source, and it is described, for a given bandwidth $\Delta\omega$, by:

$$\frac{dI^i_{\mathrm{bunch}}}{dr} \approx N_e^2\int_{\Delta\omega}\frac{d^2I^i_e}{d\omega dr}F_z(\rho(z),\omega)D(\omega)T(\omega)d\omega\,, \tag{3}$$

where N_e is the number of particles in the bunch, $d^2I^i_e/d\omega dr$ is the image distribution for a single electron, $\Delta\omega$ is the bandwidth, $T(\omega)$ is the added transmittance/reflectance of the optical elements and propagation, and $D(\omega)$ is the detector response.

Figure 1 presents the schematic of the monitor prototype. Two off-axis parabolic mirrors (OAPs) are used to image

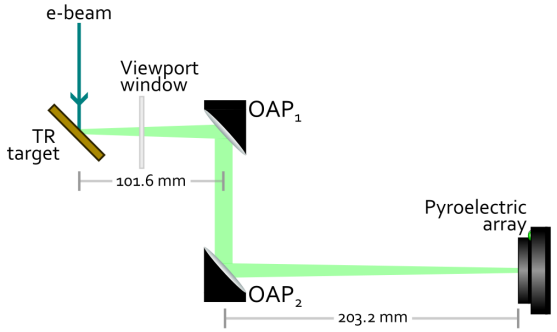

Figure 1: CTR imaging system layout.

the source of the CTR distribution by placing OAP_1 at the reflected focal length (RFL = 101.6 mm) of the center of the

transition radiation (TR) target. The second mirror, OAP_2, is placed in the anti-symmetric configuration, thus obtaining the spatial image at its RFL = 203.2 mm. The ratio of the RFLs determines the magnification, in this case, a 2x magnification.

For a more extensive description of the monitor's working principle and design process, see [8].

Zemax OpticStudio SIMULATIONS

The simulated images analyzed in this work were obtained using Zemax OpticStudio 2025/R2.

Simulation Parameters

The simulations require inputting some beam parameters and optical system properties. For the beam parameters, the beam energy is set to 3 GeV, and the charge can be disregarded, as it would only scale the intensity of the final image. The target diameter is 25 mm and placed at 45° incidence. $T(\omega)$ groups the transmittance coefficients of the window (high-resistivity float zone silicon HRFZ-Si) and the reflectance of the mirrors (protected silver), while $D(\omega)$ will be the pyroelectric array response. For the results shown in this contribution, a slight mirror misalignment has been introduced in the simulations, with a 0.4° rotation, to study the monitor's performance under realistic conditions where misalignments are possible. More detailed discussion about the role and effects of the parameters listed above on the monitor can be found in [8]; they have been carefully selected for the study of bunches $\tau_{FWHM} = [10 - 100]$ fs.

Generation of the Images

To obtain the final CTR images, the spectral data (one image per simulated frequency) are generated first, representing the image distribution of a single electron in Eq. 3. For the specific set of parameters described above, the resulting peak irradiance at the detector as a function of frequency is shown in Fig. 2, highlighting that high-frequency components (shorter bunches and shorter bunch-profile features) will dominate the final CTR images over low-frequency components.

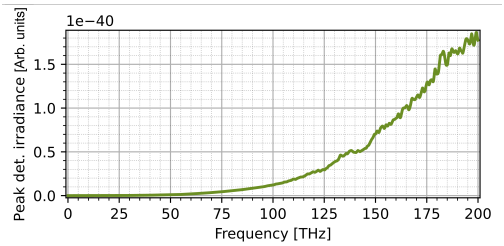

Figure 2: Peak detector irradiance vs. frequency from simulations.

This data needs to be generated only once, but it is the most time-consuming part of the process. Once the spectral data is available, the full image distribution can be computed using Eq. 3 for a given bunch profile that is within the expected bunch lengths resolved by the designed monitor.

EXPLORATION OF THE IMAGE FEATURES

Three scenarios are analyzed in this work and are presented below.

The first set of simulations is shown in Fig. 3. The bunch profiles are generated as purely Gaussian profiles in the range $\tau_{FWHM} \approx [10 - 100]$ fs. In this figure (and the subsequent ones), for each profile, the apparent bunch length is reported on the top row by two measures. τ_{FWHM} is the full width at half maximum of the distribution, but $\sqrt{m_2}$ is calculated from the second moment as a measure of how spread out the signal "mass" is along the time axis.

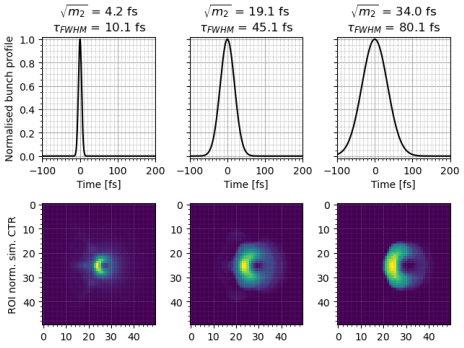

Figure 3: Images generated for purely Gaussian profiles.

The second set of simulations were produced for a main peak of 55 % of the total amplitude at fixed $\tau_{FWHM\text{-peak}}$ =15 fs and a tail of 45 % of the total amplitude, in the range $\tau_{FWHM\text{-tail}} \approx [0 - 120]$fs, and with an offset of $\sigma_{\text{tail}}/2$. The goal is to observe how the presence of (lateral) tails in the bunch can affect the output image, even though the main peak is expected to dominate, as it is a high-frequency component. It is shown in Fig. 4.

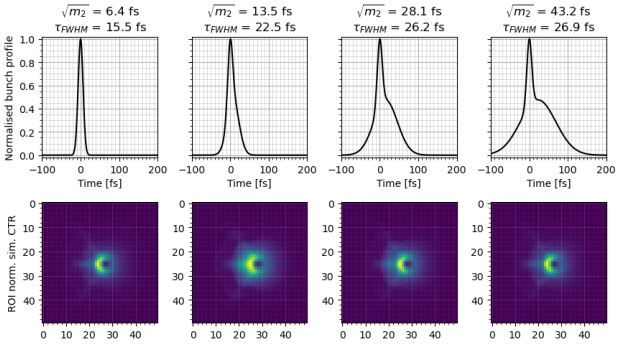

Figure 4: Images generated for a fixed main peak and a growing tail/background.

For the last set of simulations, the goal is to study small bumps/features in bunch profiles that correspond to high-frequency features, even though they have small amplitudes, and how they can affect the output CTR image. The main peak is set to 30 % of the total amplitude at fixed $\tau_{FWHM\text{-peak}}$ =20 fs and the secondary peak to 70 % of the total amplitude, in the range $\tau_{FWHM\text{-tail}} \approx [0 - 100]$fs, and with an offset of $\sigma_{\text{secondary}}$. It can be seen in Fig. 5.

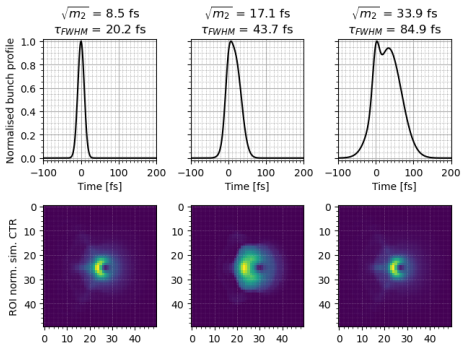

Figure 5: Images generated for a profile composed of two Gaussians (one fixed and one growing) for obtaining two peaks.

The results of the image analysis for the three cases are shown in Fig. 6. For the CTR image analysis, the *FWHM* in both image directions is used as a simple measure of the changes. High-frequency image components are closer to the center, while low-frequency components appear further away from it. The image at the source is circular and symmetrical; however, natural geometric aberrations in the OAP mirrors introduce distortions. The distortion is treated as an additional feature in this work, providing extra information about the bunch profile rather than as a shortcoming.

In each case, it should be noted that even though the apparent bunch length is kept within a similar range (see $\sqrt{m_2}$ in TDS: reference [fs]), the features within the bunch are different, and the resulting CTR images capture these differences in different ways. For Gaussian profiles in Fig. 6 (a), initially there is a steady and proportional growth in both directions of the CTR image, eventually starting to decrease in the horizontal direction for longer bunches. It can be best observed in Fig. 3, where the left side of the CTR images gets much brighter in comparison with the right side when increasing the bunch length.

In the case of Fig. 6 (b-c), there is an increase in the CTR image size when the effective bunch length starts to grow, while the spectral intensity is comparable between the high-frequency peak component and the tail or secondary bunch. It starts to decrease shortly after, as the tail and secondary peak lengthen, because the high-frequency components of the peak become dominant. It should be noted that this monitoring method does not provide any phase information about the particle distribution, meaning that in the case of Fig. 6 (b-c), a mirrored profile would produce exactly the same CTR image.

It is evident that the relationships are nonlinear and difficult to capture with a regression model, making deep learning models an interesting alternative to try next. Using both simulated and experimental data, to make full use of the proposed monitor capabilities, with architectures such as convolutional neural networks that can capture image information.

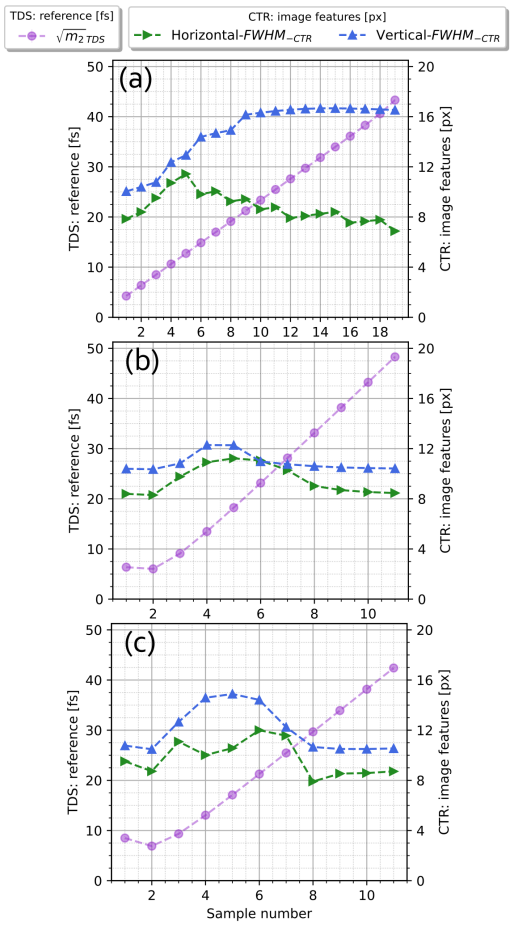

Figure 6: Image analysis results for the proposed simulation experiments (a) growing Gaussian profiles, (b) main peak and growing (lateral) tail, and (c) introduction of high-frequency features of small amplitude.

CONCLUSION

Spatial CTR images were studied from a simulation-based perspective. The simulations are a valuable source of information for developing this monitor, as they enable testing its capabilities across a wide range of particle distributions that may not be available experimentally. The image analysis shows that the CTR spatial images are complex and result from a combination of factors in the particle distribution, making them difficult to generalize with a simple regression model. Next steps include testing these detailed simulations and experimentally acquired images with deep learning models better suited to this specific problem to reconstruct the bunch profile.

ACKNOWLEDGEMENTS

This project has received funding from the European Union's Horizon Europe research and innovation program under grant agreement no. 101073480, UKRI guarantee funds, and grant agreement no. 101188004; the Cockcroft Institute core grant no. STFC ST/V001612/1; and the AWAKE-UK phase II project funded by STFC under grant no. ST/X005208/1.

REFERENCES

[1] M. C. Downer *et al.*, "Diagnostics for plasma-based electron accelerators", *Rev. Mod. Phys.*, vol. 90, no. 3, p. 035002, 2018. doi:10.1103/RevModPhys.90.035002

[2] D. V. Karlovets and A. P. Potylitsyn, "Universal description for different types of polarization radiation", *arXiv Preprint*, 2009. doi:10.48550/arXiv:0908.2336

[3] O. Zarini *et al.*, "Multioctave high-dynamic range optical spectrometer for single-pulse, longitudinal characterization of ultrashort electron bunches", *Phys. Rev. Accel. Beams*, vol. 25, no. 1, p. 012801, 2022. doi:10.1103/PhysRevAccelBeams.25.012801

[4] B. Schmidt *et al.*, "Benchmarking coherent radiation spectroscopy as a tool for high-resolution bunch shape reconstruction at free-electron lasers", *Phys. Rev. Accel. Beams*, vol. 23, no. 6, p. 062801, 2020. doi:10.1103/PhysRevAccelBeams.23.062801

[5] T. J. Maxwell *et al.*, "Coherent-radiation spectroscopy of few-femtosecond electron bunches using a middle-infrared prism spectrometer", *Phys. Rev. Lett.*, vol. 111, p. 184801, 2013. doi:10.1103/PhysRevLett.111.184801

[6] J. Wolfenden *et al.*, "Coherent transition radiation spatial imaging as a bunch length monitor", in *Proc. IPAC'19*, Melbourne, Australia, May 2019, pp. 2713–2716. doi:10.18429/JACoW-IPAC2019-WEPGW095

[7] A. G. Shkvarunets and R. B. Fiorito, "Vector electromagnetic theory of transition and diffraction radiation with application to the measurement of longitudinal bunch size", *Phys. Rev. ST Accel. Beams*, vol. 11, no. 1, p. 012801, 2008. doi:10.1103/PhysRevSTAB.11.012801

[8] A. Guisao-Betancur *et al.*, "Designing a femtosecond-resolution bunch length monitor using coherent transition radiation images", *Instruments*, vol. 9, no. 4, pp. 1-15, 2025. doi:10.3390/instruments9040029

[9] M. Castellano *et al.*, "Effects of diffraction and target finite size on coherent transition radiation spectra in bunch length measurements", *Nucl. Instrum. Methods Phys. Res. A*, vol. 435, pp. 297-307, 1999. doi:10.1016/S0168-9002(99)00566-5